EUROFUSION WPPMI-PR(15) 13473

H Lux et al.

Impurity Radiation in DEMO systems modelling

Preprint of Paper to be submitted for publication in
Fusion Engineering and Design

This work has been carried out within the framework of the EUROfusion Consortium and has received funding from the Euratom research and training programme 2014-2018 under grant agreement No 633053. The views and opinions expressed herein do not necessarily reflect those of the European Commission.

Impurity Radiation in DEMO systems modelling

H. Lux[a], R. Kemp[a], D. J. Ward[a], M. Sertoli[b]

[a] *CCFE, Culham Science Centre, Abingdon, Oxon, OX14 3DB, UK*
[b] *Max-Planck-Institut für Plasma Physik, D-85748 Garching, Germany*

Abstract

For fusion reactors with ITER divertor technology, it will be imperative to significantly reduce the heat flux into the divertor e.g. by seeded impurity radiation. This has to be done without affecting the accessibility of a high performance scenario. To assess the implications of seeded plasma impurities on DEMO design, we have developed a physically motivated, predictive impurity radiation model for radiation inside the separatrix. Evaluating the validity of our model, we find the assumption of a local ionisation equilibrium to be appropriate for our purposes and the assumption of flat impurity profiles - even though not satisfactory - to represent the best currently possible. Benchmarking our model against other codes highlights the need to use up to date atomic loss function data.

From the impurity radiation perspective, the main uncertainties in current DEMO design stem from the lack of confinement and L-H-threshold scalings that can be robustly extrapolated to highly radiative DEMO scenarios as well as the lack of appropriate models for the power flow from the separatrix into the divertor that include radiation in the scrape off layer. Despite these uncertainties in the model we can exclude that significant fuel dilution through seeded impurities (with $Z \geq Z_{Ar}$) will be an issue for DEMO, but the controllability of highly radiative scenarios still needs to be coherently shown.

Keywords: Fusion Reactor, DEMO, Systems Studies, Radiation

1. Introduction

Future generations of commercial fusion power stations including demonstration power plant reactors like DEMO will operate at significantly higher heating powers (alpha and auxiliary) than current machines. In current baseline designs, the expected heating power of DEMO is of order 500 MW [1]. To keep the heat loads on the divertor within acceptable limits ($\lesssim$ 10MW m^{-2} for current divertor technology [1]) the power passing into the scrape-off layer (SoL) and then into the divertor has to be reduced. One way of achieving this is by deliberately seeding impurities into the plasma that cool the plasma before it hits the divertor target [2]. Changing the divertor design would be an alternative solution to this exhaust problem [3, 4]. Unfortunately, currently no alternative designs with the required technology readiness level exist that can be relied upon in DEMO design studies at this stage.

Modelling future power plants like DEMO as part of conceptual design studies is the task of system codes like PROCESS [5, 6]. They provide efficient ways to finding optimal power plant designs obeying physical laws and engineering restrictions. To model the constraints from the divertor protection more accurately we have updated our impurity radiation model with respect to the description given in [7]. Especially in extrapolating from current machines to future reactors it is important that the known model uncertainties are evaluated and their influence on the derivation of design points is well understood. Therefore, it is necessary to have a predictive, physically well motivated model for impurity radiation for DEMO design activities.

Impurity radiation in the plasma can affect reactor design in several ways: Negatively, if the seeded impurities dilute the fusion fuel and if the radiation brings the power crossing the separatrix close to critical values for the L-H-threshold, as well as positively by reducing the heat loading onto the divertor. In design point studies these counteracting effects are balanced against each other to find an optimal design point. As part of these studies, it is therefore crucial to evaluate the sensitiv-

Email address: Hanni.Lux@ccfe.ac.uk (H. Lux)

[1] The current pulsed and steady-state DEMO baseline reference designs can be found at the Eurofusion IDM under https://idm.eurofusion.org/?uid=2MEYUD

ity with respect to model uncertainties that can influence the derivation of such a design point. From these assessments we can then advise essential next steps in improving conceptual reactor design models.

In section 2, we describe the implementation of our impurity radiation model (2.1) as well as its limitations (2.2). We present the benchmarking results with several other codes in 3 and show the effects of impurity radiation on DEMO design in 4. We summarise our results and conclude in section 5.

2. Model

In this section we describe the updated impurity radiation model in the PROCESS systems code. We first discuss the detailed implementation of the model (2.1) and then its range of validity (2.2). Note that this model only describes radiation from within the separatrix. Radiation from the scrape-off-layer region as well as radiation from within the divertor is currently not being modelled (c.f. discussion in 2.2.2).

2.1. Implementation

2.1.1. Electron Temperature and Density Profiles

To best capture the form of plasma profiles with an H-mode transport barrier, we follow [8] in their parametrisation of pedestal profiles for both the density

$$n(\rho) = \begin{cases} n_{ped} + (n_0 - n_{ped})\left(1 - \dfrac{\rho^2}{\rho_{ped,n}^2}\right)^{\alpha_n} \\ \qquad \text{for } 0 \le \rho \le \rho_{ped,n}, \\ n_{sep} + (n_{ped} - n_{sep})\left(\dfrac{1-\rho}{1-\rho_{ped,n}}\right) \\ \qquad \text{for } \rho_{ped,n} < \rho \le 1, \end{cases} \tag{1}$$

and temperature

$$T(\rho) = \begin{cases} T_{ped} + (T_0 - T_{ped})\left(1 - \dfrac{\rho^{\beta_T}}{\rho_{ped,T}^{\beta_T}}\right)^{\alpha_T} \\ \qquad \text{for } 0 \le \rho \le \rho_{ped,T}, \\ T_{sep} + (T_{ped} - T_{sep})\left(\dfrac{1-\rho}{1-\rho_{ped,T}}\right) \\ \qquad \text{for } \rho_{ped,T} < \rho \le 1, \end{cases} \tag{2}$$

where $\rho = r/a$ is the normalised radius and subscripts 0, *ped* and *sep*, denote values at the centre ($\rho = 0$), the pedestal top ($\rho = \rho_{ped}$) and the separatrix ($\rho = 1$), respectively. The density and temperature peaking parameters α_n and α_T as well as the second exponent β_T in the temperature profile can be chosen freely by the user.

Even though constraints on the temperature or density gradients can be found in experiments [9] none are currently implemented in PROCESS. A consistent implementation of these constraints is planned for the future and is currently in preparation.

The fuel ion temperature T_I and the electron temperature T_e in PROCESS are allowed to differ even though this feature is not typically used. In this work, we assume that the impurities are always in thermal equilibrium with the electrons. Given the other limitations of our model, we consider this a reasonable assumption.

Please note, that while the temperature and density profiles in PROCESS have pedestals, the plasma current profiles have a parabolic shape. This simplification has been made, as fully self-consistent current profiles that include the bootstrap current are difficult to describe by simple models. On the other hand, the current profile only influences the profile for the safety factor q and the fraction of the bootstrap current (with the exception of the PROCESS implementation of the Sauter-Angioni-bootstrap model [10, 11] that is mainly using the pressure profiles rather than the current profiles) and, hence, for pulsed machines only has limited influence on the overall reactor design. Therefore, this simplification should not have a significant effect on PROCESS results. Of course in steady state machines that significantly rely on high bootstrap fractions it is therefore recommended to use the Sauter-Angioni-bootstrap model.

2.1.2. Plasma Composition

Within PROCESS we assume quasi-neutrality of the plasma i.e.

$$n_e = n_I + 2n_e f_\alpha + n_e f_{beam} + \sum_i Z_i n_e f_i \tag{3}$$

where the electron number density n_e equals the sum of the fuel ion density n_I, the α-particle density $n_\alpha = n_e f_\alpha$, the beam ion density and the individual impurity densities each multiplied with their respective atomic charge. Therefore, f_α is the fraction of α-particles with respect to the electron density, f_{beam} is the fraction of the beam ions and the impurities each have a radially constant fraction f_i with respect to the electron density. For a discussion of the validity of this approach please see section 2.2.3.

While the temperature dependent average atomic charge data is available within PROCESS, when calculating the fuel ion density n_I based on eq. 3 we assume that each impurity species is fully ionised. This can be justified as the contribution of a few electrons more or less from the impurity species does not have a significant effect.

The impurity species currently implemented in PROCESS are Be, C, N, O, Ne, Si, Ar, Fe, Ni, Kr, Xe and W. All are allowed to be present in the plasma at the same time. However, for simplicity PROCESS currently allows only one seeded impurity species to be an iteration variable when optimising the amount of seeding used for divertor protection. All other impurities present are assumed to be sputtered and have a fixed fraction.

Please note that at this stage we are not making any assumptions about what type of impurities (both sputtered and seeded) will be present in DEMO or what kind of concentration we typically expect for them. Determining this will have to be part of future work, but mainly outside the scope of systems studies.

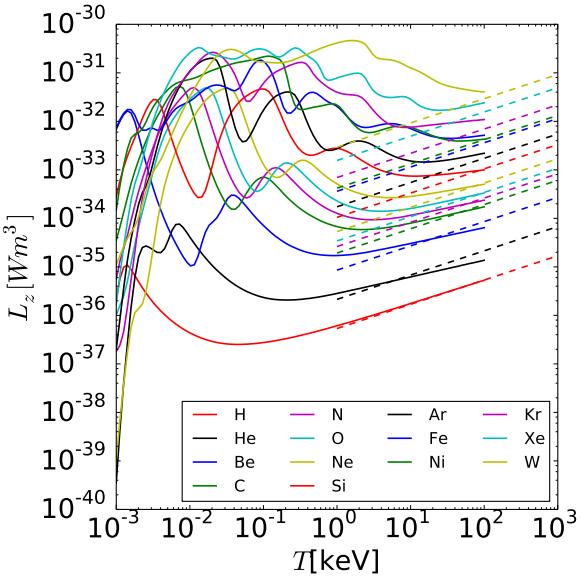

Figure 1: Loss function data from the ADAS data base (solid lines) for the different elements implemented in PROCESS (c.f. Section 2.1.3). (Due to the limited colour scheme, all colours have been used twice. Please note, that the ordering in the legend corresponds to the ordering of the atomic charges and therefore the lowest red line represents hydrogen, while the highest yellow line represents tungsten.) The dashed lines show the Bremsstrahlung radiation as given by equation 5.

2.1.3. Line and Recombination-Induced Radiation

To estimate the losses from line and recombination-induced radiation, we use the loss function data $L_z(Z_i, T)$ from the ADAS database[2] and subtract the Bremsstrahlung contribution with the analytic formula described in Section 2.1.4. Both are shown in Figure 1. The loss function data is derived assuming a local ionisation equilibrium for the fuel ions as well as the seeded and sputtered impurity species. We discuss the validity of this assumption in Section 2.2.1.

The ADAS loss function data for H, He, Be, C, N, O, Ne and Si has been produced using the generalised collisional radiative theory approach detailed in [12]. For Ni the ionisation and recombination-induced radiation data is given in [13] while for Fe data from [14] is used. These rates have a finite density dependence imposed following the procedure in [15]. The data has therefore been created using a typical electron density of $10^{19} m^{-3}$. The radiated power data is baseline ADAS data generated from ADAS codes ADAS408 described in the ADAS user manual [16]. For both Kr and Xe the ionisation and recombination rates as well as the radiation are also derived from the ADAS408 baseline. The W loss function data [17] is based on ionisation data from a configuration averaged distorted wave calculation [18] and modified ADPAK recombination data [19] combined with radiation data [19, 17] at each ionisation stage from the Cowan code using the plane-wave Born approximation. This will be kept up to date with recent developments in the field in the future.

Based on a given electron temperature and density profile as well as the radiation loss functions the total radiative power inside the separatrix and excluding the synchrotron radiation of each impurity species is given by

$$P_i = \int_V n_i(\rho) n_e(\rho) L_z(Z_i, T) dV \tag{4}$$

where $n_i = f_i n_e$. As a first approximation, the impurities are modelled assuming a constant fraction $f_i(Z)$ with respect to the electron density n_e. For a full discussion about the validity of this approximation see the discussion in Section 2.2.3.

2.1.4. Bremsstrahlung

The Bremsstrahlung radiation is already included in the ADAS loss function data. However, to distinguish it from the line and recombination induced radiation data as well as to extrapolate the loss functions at high temperatures we use an analytical description of Bremsstrahlung radiation as given by the non-relativistic Born approximation [8]

$$P_{B,i} = 5.355 \times 10^{-37} \int_V n_i n_e Z_i^2 \sqrt{T}\, dV. \tag{5}$$

[2] www.adas.ac.uk; open.adas.ac.uk

This means that the total Bremsstrahlung radiation is given by

$$P_B = \sum_i P_{B,i} = 5.355 \times 10^{-37} \int_V n_e^2 Z_{\text{eff}} \sqrt{T}\, dV \quad (6)$$

In these equations, we assume each impurity species to be fully ionised. This can of course be significantly wrong at lower temperatures and especially for high Z impurities. However, apart from informative output we are only using this formula for the high temperature ($T_e > 100\,\text{keV}$) extrapolation of the ADAS data, where it is a good approximation for total radiation for most elements (c.f. Fig.1). Therefore, this does not affect typical DEMO reactor design. It is necessary to have this kind of consistent radiation extrapolation at higher temperatures, because the optimisation routine might explore this part of the parameter space not because we think these are expected peak temperatures in a DEMO like reactor.

Please note, that the Bremsstrahlung extrapolation does not match up perfectly with the ADAS data for all elements. This is due to the simplicity of our Bremsstrahlung model that neglects e.g. relativistic and quantum mechanical effects like the Gaunt-factor. The ADAS model is significantly more complex and accurate and is therefore the main source of our radiation data.

2.1.5. Synchrotron Radiation

The model for synchrotron radiation in PROCESS has not changed from the description in [6]. It is currently following the description given in [8] based on [20, 21] who assume parabolic plasma profiles with $\beta_T = 2$ and no pedestal. Please note that the radial integration for the synchrotron radiation is quite complex and therefore only the total synchrotron radiation is calculated in the code rather than a local profile. However, as the synchrotron radiation scales with the temperature its contribution to the local radiation is only expected to be relevant in the very core of the plasma.

2.1.6. Confinement

PROCESS can use a range of different confinement scalings from the literature e.g. ITER- 98(y,2) [22]. However, as has been pointed out by [23] it is uncertain whether any of these can be used for extrapolation to highly radiative plasmas, as highly radiative scenarios have typically been excluded in the derivation of these scalings and even in the radiative scenarios included in the scaling none of the radiation is coming from the 'core region' of the plasma. As a first step to address this issue, one can subtract expected 'instantaneous' radiation losses from the heating power in the conducted loss power $P_L = P_H - P_{rad,inst}$ calculation. We assume this affects both the definition of the confinement time as the ratio of the stored energy and the loss power $\tau = W/P_L$ as well as the loss power in the confinement scalings $\tau_E(98, y, 2) \propto P_L^{-0.69}$. Therefore, in PROCESS both times the loss power is given by

$$P_L = P_{aux} + P_\alpha + P_{charge} + P_{ohm} - P_{rad,core}, \quad (7)$$

where P_{aux} is the total auxiliary heating, P_α is the α-heating power, P_{charge} is the non-α charged particle fusion power (if other forms of fusion reactions are assumed), P_{ohm} is the ohmic heating and $P_{rad,core}$ the radiative power within a user defined core radius ρ_{core}. This assumes that the radiative losses within ρ_{core}

$$\begin{aligned} P_{rad,core} &= P_{sync} \\ &+ V \int_0^{\rho_{core}} 2 n_i n_e L_z(Z_i, T) \rho d\rho, \end{aligned} \quad (8)$$

are instantaneous losses as discussed above. (Here the synchrotron radiation P_{sync} is assumed to only come from the core region and V is the plasma volume.) For a full discussion why we consider this type of radiation correction to be the most appropriate approach given the current data and modelling see [24]. How this effects DEMO design considerations is discussed in Section 4.1.

In the following, we will define everything as edge radiation that is radiated within the separatrix, but not counted as core radiation given by 8

$$P_{rad,edge} = P_{rad,sep} - P_{rad,core}. \quad (9)$$

Within PROCESS it is also possible not to correct the loss power for radiation at all, but this option is not used within this work. To show the difference between the radiation corrected and the non-radiation corrected confinement, per default PROCESS outputs two different definitions of the H-factor. The definition used in the design of the machine is the radiation corrected version

$$H = \frac{W}{P_L \tau_{scaling}(P_L)} \quad (10)$$

where W is the total plasma energy calculated from the density and temperature profiles, P_L is given by equation 7 and $\tau_{scaling}$ is the user defined version of the confinement scaling. In contrast, the non radiation corrected version is given by

$$H^* = \frac{W}{P_H \tau_{scaling}(P_H)} \quad (11)$$

where the heating power is given by $P_H = P_{aux} + P_\alpha + P_{charge} + P_{ohm}$. This is the quantity typically calculated for experimental data.

2.1.7. Power balance and constraints

To assure physical consistency within PROCESS several power balance equations have been implemented. Apart from a global power balance also the individual power balances of electrons and ions can be enforced. The global power balance assures that

$$\frac{3\overline{nT}}{\tau_E} + P_{rad,core} = P_\alpha + P_{charge} + P_{ohm} + P_{aux} \quad (12)$$

where $\overline{nT}$ is the product of the average density and temperature, $P_{rad,core}$ is the core radiation as defined by eq. 8.

Despite the 1d density and temperature profiles in PROCESS we are not enforcing a local power balance, as we currently have no local model for the different heating sources implemented in PROCESS. However, a further global constraint ensures that not more power can be radiated away than is deposited in the plasma. This places an upper limit on the allowed total radiation power inside the separatrix $P_{rad,sep}$.

Currently, several scalings of the L-H power threshold at the separatrix are calculated within PROCESS. They are not enforced by default, but the user can choose to select them either as upper or lower bounds to enforce operation in either L- or H-mode. The options are

1. ITER 1996 nominal [25],
2. ITER 1996 upper bound [25],
3. ITER 1996 lower bound [25],
4. ITER 1997 excluding elongation [26],
5. ITER 1997 including elongation [26],
6. 2008 Martin scaling: nominal [27],
7. 2008 Martin scaling: 95% upper bound [27],
8. 2008 Martin scaling: 95% lower bound [27],

where the Martin scaling - being the most recent - is the recommended scaling to use. Please note that within PROCESS and throughout this paper we assume that the L-H-threshold values also correspond to the H-L-threshold value and that no hysteresis exists. We discuss the effect of the L-H threshold on divertor protection in DEMO in Section 4.3.

Please note, that none of the currently existing L-H threshold scalings has been based on high radiative plasma experiments. Therefore, their applicability to highly radiative DEMO scenarios is not clear.

If divertor protection for DEMO is enforced in the code, P_{sep}/R is constrained to lie below a user defined value (current designs assume 17 MW/m for a pulsed DEMO and 20 MW/m for a more advanced steady state DEMO), where the power across the separatrix is given by

$$P_{sep} = P_\alpha + P_{charge} + P_{aux} + P_{ohm} - P_{rad,sep}. \quad (13)$$

For a further discussion of this figure of merit see Section 2.2.2.

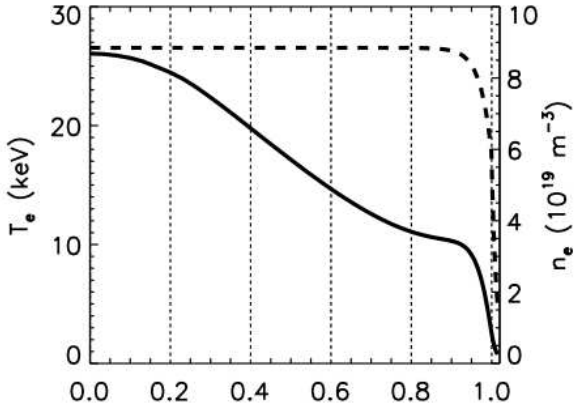

Figure 2: Electron density (dashed line, right axis) and temperature profiles (solid line, left axis) for the DEMO like STRAHL simulations evaluating the validity of the local ionisation equilibrium (LIE).

2.2. Validity Limits

In the following sections, we are discussing the major known limitations on our model validity, in which way these are affecting DEMO systems modelling and how these can possibly be improved in the future.

2.2.1. Local Ionisation Equilibrium (LIE)

The ADAS loss function data described in Section 2.1.3 has been derived assuming a local coronal equilibrium or local ionisation equilibrium. This assumption can have significant influence on the amount of radiation expected from impurities [28, 29]. In particular, it can lead to severe under- or overestimation of the radiation emitted from plasma impurities depending on the respective temperatures near the plasma edge, where typical transport times are expected to be much shorter than respective equilibration time scales due to the strong temperature gradients on the specific impurities.

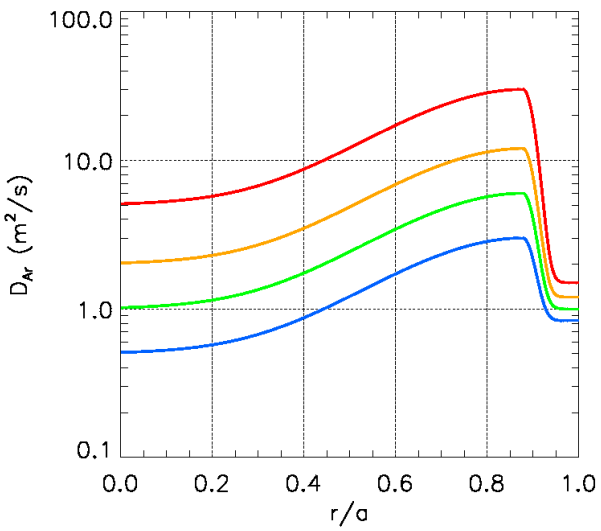

Figure 3: Range of transport coefficients used in the STRAHL simulations when evaluating the validity of the LIE.

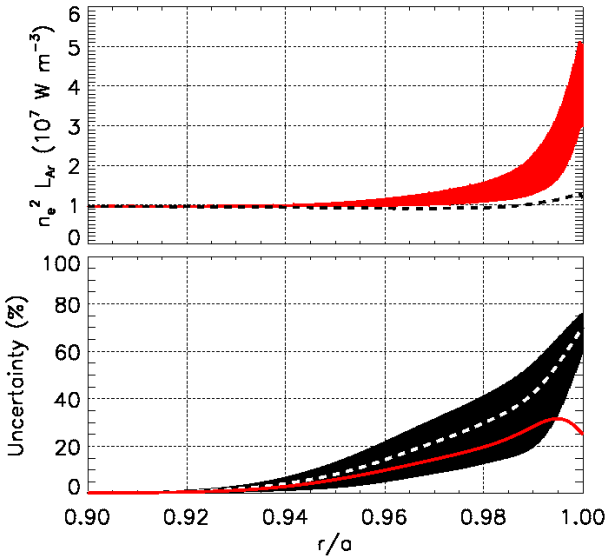

Figure 4: Argon loss functions multiplied with the electron density squared (upper plot) for STRAHL simulations with different diffusion coefficients (red band) at equilibrium. The dashed black line shows the curve assuming LIE. The lower plot shows the standard deviation of the different transport runs (red line) and the errors of the LIE run with respect to the transport runs (white-black dashed line = mean, black band = upper and lower boundaries). Note, that both plots only show $\rho > 0.9$ where the main differences occur.

However, in this region there are two competing effects: If the respective impurity is not already fully stripped at lower temperatures, then strong temperature gradients will lead to a strong deviation from LIE, but will only affect a small plasma volume. On the other side, shallow temperature gradients affect the plasma in a larger volume, but cause smaller deviations from LIE. To evaluate the maximum error introduced by this assumption on the total radiation from within the separatrix, we need to systematically analyse the transition between both regimes.

Using simulations by the 1D impurity transport code STRAHL [30, 31], for a DEMO like system we have investigated the effect of varying transport parameters.

The electron density and temperature profiles we assumed for a DEMO like system are shown in Figure 2, while we follow [32] in the range of diffusion coefficients used in our simulations as displayed in Figure 3. We have injected argon, iron and tungsten and evolved the simulations to an equilibrium. Figure 4 show the results for argon at equilibrium, which represents the worst case of the three investigated impurities. The upper plot shows a proxy for the power density $n_e^2 L_z$ that can be easily interpreted, if constant impurity fractions f_i are assumed as we do in our model. The red band shows the spread of values for assuming different diffusion coefficients, while the black dashed line shows the values assuming local ionisation equilibrium. The lower plot shows the standard deviation of the values in the red band and the normalised difference of the LIE values with respect to the transport simulations (black band and dashed line). Note that both plots are zoomed into the edge region of the plasma ($\rho > 0.9$). However, even though locally the LIE assumptions causes errors of more than 70% we find that the errors on $P_{rad,sep}$ are never larger than 10% independent of the impurity species. As $P_{rad,sep}$ is the quantity we are interested in for our PROCESS runs, we can therefore conclude that LIE is a reasonable assumption for modelling radiation inside the separatrix in systems codes. This is consistent with results by [33].

We expect low-Z impurities to be fully stripped at DEMO relevant temperatures inside the separatrix and therefore they should always be in LIE. High-Z elements on the other hand have faster ionisation and recombination rates and are therefore less affected by temperature gradients than intermediate-Z elements. This suggests that despite only testing 3 impurities this result will hold true for all relevant impurity species.

Unfortunately, these deviations from LIE are not systematic and therefore cannot be corrected for, as they depend on the variation of the respective cooling curve around the pedestal temperature. However, $P_{rad,core}$ is the quantity that is more relevant for reactor design than

$P_{rad,sep}$ and is expected to have negligible errors for $\rho_{core} < 0.9$.

2.2.2. Scrape-off-Layer/Divertor

At this stage no robust model for the power flow from the separatrix via the scrape-off-layer (SoL) into the divertor as well as the expected impurity radiation from these regions exists, in particular not for highly radiative, DEMO relevant plasmas. To allow for accurate modelling of the radiation from these regions in the future, a series of dedicated experiments and modelling will be necessary.

Given the lack of a more detailed model, we instead use P_{sep}/R as a figure of merit for divertor similarity, where P_{sep} is the conducted power that crosses the separatrix (see definition in eq. 13) and R is the major radius of the device (c.f. e.g. [3, 4]).

This figure of merit has originally been motivated by including atomic physics in similarity arguments for divertor modelling in magnetic confinement devices [34]. As recent experiments indicate that the scrape-off-layer width scales independently of the major radius of the device $\lambda_q \propto R^0$ [35] and, therefore, the wetted area of the divertor scales linearly with R, this is a strong argument that extrapolations of divertor conditions scale with P_{sep}/R instead of P_{sep}/R^2 or P_{sep}/R^3.

To estimate what values of P_{sep}/R allow safe divertor heat loading in DEMO, we assume that ITER will be capable of safely operating with $P_{sep}/R \sim 15\,\mathrm{MW/m}$, which is required to operate above the L-H power threshold [36]. So far the maximum experimental value has been achieved on ASDEX Upgrade with $P_{sep}/R = 10\,\mathrm{MW/m}$ with a time averaged peak heat flux at the outer divertor target of about $5\,\mathrm{MW/m^2}$ [37]. As this is well below the material limit for ITER-like divertors of $10\,\mathrm{MW/m^2}$ [1], it is suggested that safe divertor operation at $P_{sep}/R \sim 15\,\mathrm{MW/m}$ is not unrealistic. For DEMO one can therefore argue that at least similar values should be achievable, even though the higher neutron load in the DEMO divertor might in practice reduce the material limits with respect to ITER. Assuming that the value of 15 MW/m is not corresponding to the achievable upper limit, we optimistically assume that we can safely reach values of 17 MW/m in a pulsed DEMO and 20 MW/m in a more advanced steady state DEMO. However, without experimental confirmation this values should be taken to have at least an uncertainty of $\pm 5\,\mathrm{MW/m}$.

However, while we can use P_{sep}/R as a figure of merit for divertor protection, it does not give a robust measure of the heat flux onto the divertor. This severely restricts the availability modelling for the divertor in PROCESS, which is directly dependent on both the heat flux as well as the neutron load on the divertor. This in turn has a direct effect on the overall power plant design and costs. It will be therefore essential in the future to improve the model of the heat load on the divertor.

2.2.3. Flat Impurity Profiles

Currently we assume that the impurity density profiles can be described by the electron density profile multiplied by a constant impurity fraction f_i as recommended in the ITER Physics Design Guidelines [38]. Even though it has been suggested that these kind of models should be replaced with more realistic approaches [23], predictions for the impurity transport in DEMO are at the current stage rather uncertain [39] and therefore, such flat impurity profiles are a good compromise between the two possible extremes of hollow or peaked impurity density distributions. Furthermore, current experiments indicated that in typical H-mode plasmas this is not a too bad assumption. This is because the gradients in impurity density profiles caused by turbulent transport are small in comparisons to typical gradients in transport barriers [40, 41].

A possible caveat is the difference in fuelling strategies between current experiments and reactors i.e. gas puffing instead of pellet fuelling, where the effects on impurity profiles have not yet been investigated.

For an evaluation of the effect of hollow impurity profiles on our results see the comparison with JETTO simulations in Section 3.3.

2.2.4. 1D Profiles and Scenario Stability

Our model is designed to be simple to allow for large parameter scans within the total power plant design. This means that any poloidally or toroidally asymmetric radiation cannot be described. As a consequence, radiation around the X-point as typically seen in current experiments cannot be reproduced in our model. Therefore, we might be underestimating the total radiation power in the machine.

Furthermore, the effect of multifaceted asymmetric radiation from the edge (MARFEs, [42]) that are often seen in impurity seeded experiments, cannot be taken into account in our modelling. In turn, this also means that - while we assure the correct global power balance within our code - there is no guarantee that the resulting operating scenario cannot be unstable with respect to local effects like e.g. unstable MARFEs. Therefore, it is necessary to follow up any PROCESS design point analysis with scenario modelling to verify the viability of the result. Furthermore, strong interactions with current

	PROCESS	Sycomore
f_{He}	11 % (input)	11 %
f_{Ar}	0.5 % (input)	0.5 %
P_{brems}	147 MW	144 MW
P_{line}	102 MW	152 MW

Table 1: Table of PROCESS - Sycomore benchmarking values. The helium and argon fractions are input parameters in PROCESS and are therefore the same by default. The Bremsstrahlung power is in good agreement, but the power in line and recombination radiation differs significantly due to different ADAS data used.

experiments are necessary to be aware of any further limitations of our models.

3. Benchmarking

To validate our model implementation, we have conducted several benchmarking tests with other codes. The results of these tests are presented in the following sections.

3.1. The Sycomore Systems Code

The Sycomore code is another systems code developed at CEA [43]. It uses a similar radiation model with the same parametrisation for temperature and density profiles and Bremsstrahlung radiation. It also uses ADAS loss function data. When initially comparing our results to an equivalent run for a DEMO like machine with argon seeding ($f_{Ar} = 0.005$), we found that the line radiation power in PROCESS is about $1/3$ lower than in Sycomore, while the Bremsstrahlung results are the same within numerical errors. This disagreement can be fully explained by the use of older ADAS data in Sycomore [44, 15]. This shows that it is essential for these kind of physically motivated models to use up to date loss function data including the most recent developments in atomic physics. As a result, the Sycomore code has updated its loss functions to the most recent ADAS version and both systems codes plan to keep their atomic data in line with upcoming updates in the ADAS data base. However, more recent updates of the loss function data in the the ADAS database should be better converged and, therefore, future updates in the atomic data base are *not* expected to be a source of uncertainties as large as 50%.

As a guideline, in lack of more quantitative values, the intrinsic uncertainties of the ADAS data increase with the charge of the radiating impurity as well as decrease with temperature. The old data ADAS data previously used by the Sycomore code did a.o. not take the dielectric recombination into account. This is one of the main source of differences between the more recent data sets. Now that all used data sets include dielectric recombination, the uncertainties on current data sets should be significantly less than 50% suggesting that for the low to intermediate Z regime they are less or equivalent to other sources of uncertainty in our code.

3.2. The METIS Transport Code

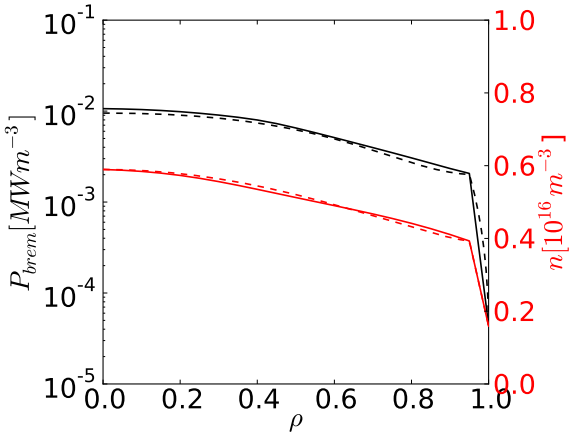

Figure 5: Comparison of the Bremsstrahlung radiation (black) and corresponding impurity density profile vs. normalised radius $\rho = r/a$ (red) for tungsten from METIS simulations (solid lines) and the PROCESS code (dashed lines). Differences between the total radiation powers are < 10%.

The METIS transport code is part of the CRONOS suite [45]. We compare the results of our radiation model with their simulations of a pulsed DEMO power plant with high impurity radiation [46]. In Figure 5, we only show the comparison of the Bremsstrahlung profiles for tungsten radiation, but in general the differences in the total line radiation as well as the total Bremsstrahlung radiation for tungsten, argon and helium between the two codes are below 10%. Unlike PROCESS METIS takes relativistic corrections for the Bremsstrahlung into account. However, given the good agreement between the results, relativistic effects do not seem to play a significant role for DEMO like machines independent of the impurity species in question. This of course does not have to be the case for higher temperature scenarios than currently anticipated.

3.3. The Jetto/Sanco Transport Code

The JETTO transport code is part of the JINTRAC suite [47]. It uses the NCLASS neoclassical transport model

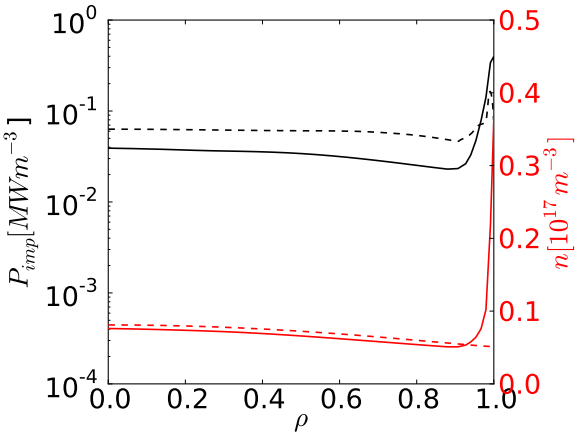

Figure 6: Comparison of the total impurity radiation (black) and corresponding impurity density profile (red) for tungsten from JETTO simulations (solid lines) and the impurity profile module in PROCESS (dashed lines).

[48] for both fuel and impurity species as well as an analytical anomalous transport model that has been scaled to match the expected plasma performance.

Figure 6 shows a comparison of the tungsten data from our PROCESS radiation model matched to JETTO simulations for a pulsed DEMO machine [46]. As our model assumes constant impurity fractions along the profile, we have matched the total impurity fraction between both codes. This leads to a slightly higher impurity density in the core region and a lower impurity density in the edge region ($\rho \gtrsim 0.9$) and therefore to a significant underestimation of the impurity radiation from the edge region in the PROCESS results in comparison to the JETTO predictions. In the DEMO simulations in this benchmark comparison the differences in the total impurity radiation are of order $\sim 20\%$ for Ar and more than $\sim 50\%$ for W. This illustrates the effect hollow impurity profiles can have on the total radiation from the plasma . However, as discussed in Section 2.2.3 unless impurity transport in DEMO like machines can be more accurately predicted, this is not something that can currently be improved in our model. Furthermore, as such strong impurity peaking at the edge is not observed in current experiments, we doubt that we are strongly underestimating the total impurity radiation from the edge in our models due to this effect.

4. Effects on DEMO design

After validating our new model, we have applied it to assess the impact of divertor protection using seeded impurity radiation on DEMO design. This section summarises our results.

Please note, that the plots shown in this section are simple variations around a single DEMO-like design point and should be seen as qualitative illustrations of critical issues in DEMO design rather than quantitative descriptions of a DEMO design. Proper design point evaluations typically scan a significantly larger parameter space and, therefore, display more complex relations. However, this work is meant to be intuitively instructive and, therefore, has been restricted to simple one dimensional parameter scans.

All results in this section have been produced using the latest master release of PROCESS (version 341). They are all based on a design close to the June 2014 steady state DEMO reference design[3] with $R = 8.5\,\mathrm{m}$, $P_{fus} \in [1.6, 2.1]\,\mathrm{GW}$ and $P_{aux} \in [110 - 130]\,\mathrm{MW}$. The temperature profiles have a fixed peak temperature of $T_0 \approx 30\mathrm{keV}$ and a fixed average temperature of $\langle T_e \rangle = 15\mathrm{keV}$. The average electron density is $\langle n_e \rangle \approx 8 \times 10^{19} m^{-3}$ which results in a line averaged density which is 1.2 times the Greenwald limit. To assure global power consistency despite the fixed internal energy the H-factor has been allowed to vary.

Please note, that none of the work in this section uses the pedestalised density and temperature profiles as we currently do not consider this model self-consistent. To assure such self-consistency is part of future work beyond the scope of this paper.

4.1. Uncertainties in Confinement Scalings

As discussed in Section 2.1.6, we assume that the existing confinement scalings can be extrapolated to high radiation scenarios by subtracting a certain part of the radiative power from the plasma core from the loss power P_L. We parametrise this core radiation power by a simple normalised cut off radius ρ_{core}. Figure 7 shows the effect of varying ρ_{core} on the H-factor (as defined by eq. 10 and the confinement time, where both the confinement time τ_E and the confinement scaling $\tau_E(98, y, 2)$ are calculated using the loss power P_L as defined in equation 7. We find that while the H-factor masks the severity of the uncertainty, the confinement time scaling is affected significantly. This emphasises the need for experimentally verified confinement scalings for highly radiative plasmas to be able to make reliable predictions for DEMO type machines as previously pointed out by [23].

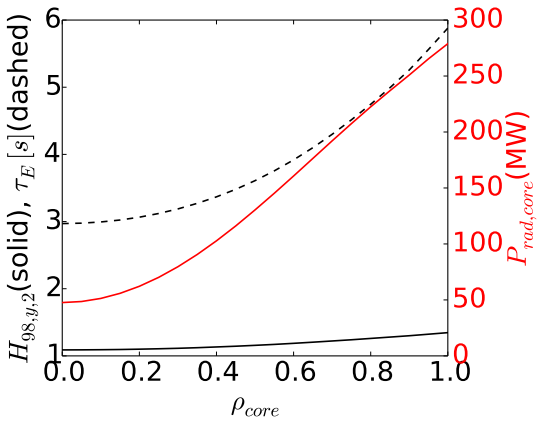

Figure 7: A scan of the cut off radius ρ_{core} of the radiation that is corrected for in the confinement scaling $P_{rad,core}$ (red solid line). The total impurity radiation has been fixed. The effect on the H-factor $H_{98,y,2}$ (solid black line) and the total energy confinement time τ_E (dashed black line) are shown.

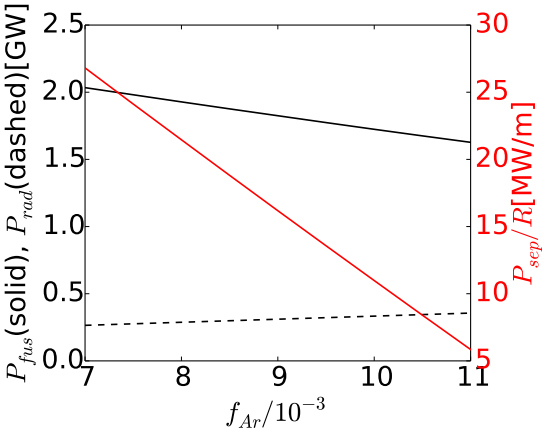

Figure 8: Varying the impurity fraction in a DEMO like machine with fixed plasma scenario. While the fusion power P_{fus} (solid black line) decreases due to fuel dilution, the total radiated power increases and reduces the heat load on the divertor P_{div}/R. Fortunately, our results suggest that achieving divertor protection is possible before significantly diluting the fusion fuel.

4.2. Fuel Dilution

One concern in DEMO design is that seeded impurities inside the separatrix will dilute the core plasma and therefore reduce the fusion power [49]. In Figure 8, we evaluate the effect of plasma dilution due to argon seeding while assuming a fixed tungsten contamination from plasma facing components of $f_W = 10^{-5}$ [17] and a helium fraction of 10%. When varying the argon fraction in a fixed plasma scenario of a steady state DEMO like machine, the fusion power decreases due to fuel dilution. However, in our example case the decrease in heat load on the divertor (P_{sep}/R) due to the increase in total radiative power is much more significant. Hence, for DEMO type systems protecting the divertor ($P_{sep}/R \lesssim 20\,\mathrm{MW/m}$) with impurity radiation is unlikely to cause any significant fuel dilution. This confirms earlier work [49] and is independent of whether a contamination of high Z impurities from plasma facing components adding to the total radiation is assumed. Due to their higher radiative powers, higher Z impurities are not expected to cause any significant fuel dilution effects. However, due to the smaller amounts necessary, they make a radiative power balance in a reactor harder to control (see also Section 4.4). This is especially true for the reduced diagnostics expected to be available on DEMO [50]. On the other hand, lower Z impurities are expected to cause stronger fuel dilution. As [51] have shown neon in the core plasma can cause significant amounts of plasma dilution. Therefore, it will be important for DEMO to choose the appropriate seeded impurity to match these constraints and argon seems a good candidate for main chamber radiation on DEMO [28]. If neon or another lower Z impurity is used for radiation in the scrape-off-layer and divertor region, it should be investigated whether this would penetrate into the core plasma or will be stopped from significantly diluting the fusion fuel in the core due to temperature screening.

4.3. L-H transition

One important issue in DEMO design is to find a design point that is robustly in H-mode assuring high plasma performance while radiating enough power from the main plasma to protect the divertor at the same time. Figure 9 illustrates this issue. It shows the power crossing the separatrix P_{sep} vs. the divertor figure of merit P_{sep}/R as discussed in Section 2.2.2. The dashed line shows the nominal value of the Martin 2008 [27] LH-threshold scaling, while the dotted lines indicate its uncertainty within 95% confidence levels. This illustrates that as for ITER, operation in H-mode for DEMO within divertor protection might be challenging. However, in the scaling law radiation has not been taken into account, this means $P_{sep} = P_H$ while we assume $P_{sep} = P_H - P_{rad,sep}$. This makes our estimate more conservative. On the other hand, the data base from which the scaling has been derived explicitly excludes experiments with significant amounts of total radiation ($P_{rad}/P_L < 0.5$, [27]) and most of the radiation in those

[3] Eurofusion IDM - EFDA_D_2L9VPW v.1.0

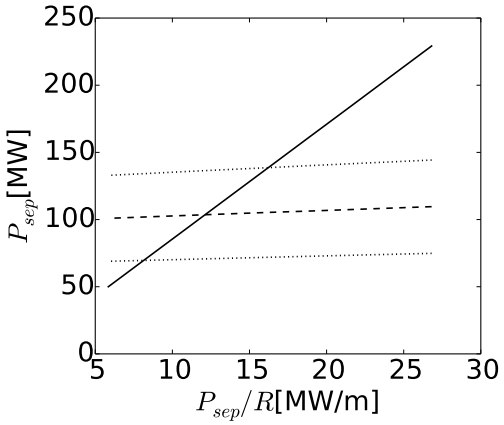

Figure 9: The black solid line shows the relation between the power leaving the separatrix P_{sep} and the figure of merit for divertor performance P_{sep}/R varying the seeded impurity fraction as in Figure 8. The dashed line shows the average ion mass dependent nominal value for the Martin 2008 LH-threshold [27], while the dotted lines show the 95% upper and lower bounds. Obviously too strong constraints on the divertor performance make operation in H-mode impossible.

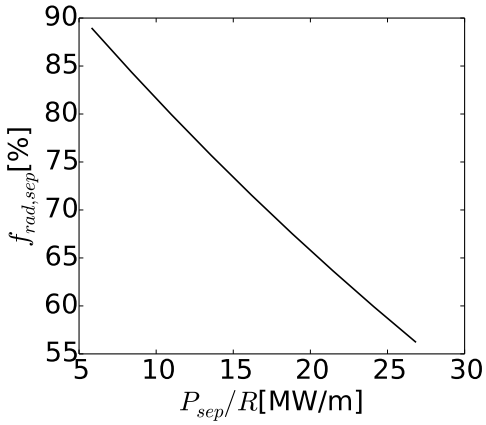

Figure 10: The plot shows the relation between the radiative fraction inside the separatrix $f_{rad,sep}$ as defined by eq. 14 and the figure of merit for divertor performance P_{sep}/R varying the seeded impurity fraction as in Figure 8. It illustrates qualitatively how enforcing smaller values of P_{sep}/R significantly increases the need for high radiative fractions inside the main plasma. Please note, that at the current stage both the values for limits on P_{sep}/R as well as achievable radiation fractions are still highly uncertain.

experiments will have come from the SoL and divertor region rather than from inside the seperatrix. Therefore, it is unclear how strongly conservative this estimate is. In general, experimental verification of these scalings in DEMO relevant high radiation scenarios seems to be important for a robust determination of DEMO design points.

4.4. Main Plasma Radiative Fractions

One open question for DEMO design is whether the high fraction of radiative power in comparison to the conducted loss power needed for divertor protection is achievable in stable reactor relevant operating scenarios. Experiments pushing to a maximal $f_{rad} = P_{rad,bol}/P_{heat}$, where $P_{rad,bol}$ is the measured total radiative power including radiation from the SoL and divertor regions, have found values on ASDEX Upgrade of $f_{rad} = 0.85 - 0.9$ with N_2 seeding [52, 53] and on JET $f_{rad} = 0.75$ with N_2 seeding as well as $f_{rad} = 0.63$ for both argon and neon seeding [54, 55]. Though the values on JET do not necessarily have to correspond to the highest possible limit.

Figure 10 shows the radiative fraction inside the separatrix as defined by

$$f_{rad,sep} = \frac{P_{rad,sep}}{P_{aux} + P_{\alpha} + P_{charge} + P_{ohm}}. \qquad (14)$$

It shows that the fraction needed for divertor protection limits is highly sensitive to the exact parameters chosen and therefore is not very well constrained. This means that with our current model, we can only make qualitative statements about required radiation fraction for DEMO operations rather than quantitative. Furthermore, the definition of $f_{rad,sep}$ differs from the definition used in experiments as given above. As our model currently does not include predictions for radiation from the divertor/SoL regions and it is difficult to experimentally distinguish between radiation inside or outside the separatrix, a more direct comparison to the experimental results is currently not possible within this framework.

The high sensitivity of the necessary radiative fraction raises another issue in DEMO design. For DEMO operations it will be crucial to be able to control the amount of impurity seeding necessary to keep the divertor heat load in acceptable limits. As this cannot be done to arbitrarily high accuracy [56], any operational point needs to be reasonably far away from any operational limits i.e. the L-H-threshold, the limit for divertor protection as well as the limit for stably operating a highly radiative plasma. These issues need to be investigated further to assure robust reactor performance including divertor protection. Also see [57] for discussion of importance of resilience and control of a DEMO operating point.

5. Conclusions

In this work, we have presented the new model for impurity radiation within the separatrix in the systems code PROCESS. It includes a parametrisation of pedestalised density and temperature profiles, assumes quasi-neutrality and constant impurity fractions in the plasma. It predicts the line and recombination induced radiation from a range of (seeded and sputtered) impurities, the fuel and the He-ash in the plasma as well as their Bremsstrahlung radiation and synchrotron radiation from the core plasma. We have, furthermore, implemented correction for high radiative scenarios to current confinement scalings based on work described in [24] and consistency checks on various options for global power balances within PROCESS.

We have assessed the severity of several limitations of the current model and found that the assumption of a local ionisation equilibrium is appropriate for modelling impurity radiation inside the separatrix within a systems code approach. This assumption is no longer valid for radiation from the SoL or divertor region. However, due to the lack of an appropriate model for the radiation in these regions, we resort to using P_{sep}/R as a figure of merit for divertor similarity and to place constraints on the overall machine design. Furthermore, as current experiments and simulations cannot robustly predict impurity profiles for DEMO type plasmas, we assume constant impurity fractions with respect to the electron density.

To validate the implementation of our model, we have run benchmarking tests against the Sycomore systems code as well as the METIS and JETTO transport codes. We find that while using up to date atomic data and assuming realistic impurity densities is quite crucial for correctly predicting impurity radiation from DEMO like plasmas, relativistic correction to the Bremsstrahlung predictions on the other hand seem unnecessary for the currently considered temperature range. Furthermore, the assumption of flat impurity profiles can lead to large errors in the radiation predictions, but is currently the best available model given the uncertainties in impurity transport.

Finally, we have applied our new radiation model to evaluate the consequences of divertor protection through seeded impurity radiation on DEMO design. Evaluating the uncertainties in extrapolating current confinement time scalings to highly radiative DEMO scenarios, we find that whether the loss power is corrected by all or none of the radiation inside the separatrix has a significant influence on the predicted confinement times for DEMO. Therefore, a robust confinement time scaling for highly radiative DEMO scenarios will be essential for future DEMO design studies. Investigating the effects of impurity seeding for divertor protection on fuel dilution, our results suggest this effect is not critical for the right choice of seeded impurities ($Z \geq Z_{Ar}$). When balancing operating above the L-H threshold against divertor protection using P_{sep}/R as a figure of merit, we find that the current uncertainties on both the L-H threshold as well as achievable values of divertor performance make it difficult to find robust DEMO design points. To consistently predict H-mode operating scenarios that do not exceed material limits for divertor head loading, more accurate models for the power flow in the SoL and divertor for high radiation plasmas as well as corresponding L-H threshold scalings for highly radiative plasmas are important. Furthermore, radiative fractions inside the separatrix are highly sensitive to safely achievable values of P_{sep}/R. This not only emphasises the importance of ongoing experiments to determine the highest achievable radiation fraction in a stable operating scenario, but raises the question of resilience of such operating points.

6. Acknowledgements

HL is grateful to Peter Knight for his help with implementing the new radiation model in PROCESS. She thanks Luca Garzotti and Damian King for helpful discussions about the JETTO/Sanco results, Jean-Francois Artaud for the help with his METIS results and Cedric Reux for his collaboration on the Sycomore results. Additionally, HL thanks Martin O'Mullane for providing her with the ADAS data and the corresponding documentation. Furthermore, she is grateful to Matthias Bernert, Ralph Dux, Fulvio Millitello, Thomas Puetterich, Matthew Reinke, Hugh Summers, Ronald Wenninger, Marco Wischmeier, Hartmut Zohm and many others for their discussions in the preparation of this work.

This work has been (part-) funded by the RCUK Energy Programme [grant number EP/I501045]. To obtain further information on the data and models underlying this paper please contact PublicationsManager@ccfe.ac.uk. Furthermore, this work has been carried out within the framework of the EUROfusion Consortium and has received funding from the Euratom research and training programme 2014-2018 under grant agreement No 633053. The views and opinions expressed herein do not necessarily reflect those of the European Commission.

References

[1] J. Linke, High heat flux performance of plasma facing materials and components under service conditions in future fusion reactors, Fusion Science and Technology 49 (2T) (2006) 455–464.

[2] G. Federici, R. Kemp, D. Ward, C. Bachmann, T. Franke, S. Gonzalez, C. Lowry, M. Gadomska, J. Harman, B. Meszaros, C. Morlock, F. Romanelli, R. Wenninger, Overview of eu demo design and r&d activities, Fusion Engineering and Design 89 (78) (2014) 882 – 889, proceedings of the 11th International Symposium on Fusion Nuclear Technology-11 (ISFNT-11) Barcelona, Spain, 15-20 September, 2013. doi:http://dx.doi.org/10.1016/j.fusengdes.2014.01.070.
URL http://www.sciencedirect.com/science/article/pii/S0920379614000714

[3] M. Kotschenreuther, P. M. Valanju, S. M. Mahajan, J. C. Wiley, On heat loading, novel divertors, and fusion reactors, Physics of Plasmas 14 (7) (2007) –. doi:http://dx.doi.org/10.1063/1.2739422.
URL http://scitation.aip.org/content/aip/journal/pop/14/7/10.1063/1.2739422

[4] M. Kotschenreuther, P. Valanju, S. Mahajan, L. Zheng, L. Pearlstein, R. Bulmer, J. Canik, R. Maingi, The super x divertor (sxd) and a compact fusion neutron source (cfns), Nuclear Fusion 50 (3) (2010) 035003.
URL http://stacks.iop.org/0029-5515/50/i=3/a=035003

[5] T. C. Hender, M. K. Bevir, M. Cox, R. J. Hastie, P. J. Knight, et al., Physics assessment for the European reactor study, Tech. Rep. AEA FUS 172, UKAEA/Euratom Fusion Association (1992).

[6] M. Kovari, R. Kemp, H. Lux, P. Knight, J. Morris, D. Ward, process: A systems code for fusion power plantspart 1: Physics, Fusion Engineering and Design 89 (12) (2014) 3054 – 3069. doi:http://dx.doi.org/10.1016/j.fusengdes.2014.09.018.
URL http://www.sciencedirect.com/science/article/pii/S0920379614005961

[7] C. Lowry, L. Garzotti, T. Hartmann, I. Ivanova-Stanik, J. Johner, et al., Activity 4, divertor physics, Tech. rep., UKAEA/Euratom Fusion Association (April 2012).

[8] J. Johner, Helios: A zero-dimensional tool for next step and reactor studies, Fusion Science and Technology 59 (2) (2011) 308–349.

[9] C. Angioni, E. Fable, M. Greenwald, M. Maslov, A. G. Peeters, H. Takenaga, H. Weisen, Particle transport in tokamak plasmas, theory and experiment, Plasma Physics and Controlled Fusion 51 (12) (2009) 124017.
URL http://stacks.iop.org/0741-3335/51/i=12/a=124017

[10] O. Sauter, C. Angioni, Y. R. Lin-Liu, Neoclassical conductivity and bootstrap current formulas for general axisymmetric equilibria and arbitrary collisionality regime, Physics of Plasmas (1994-present) 6 (7) (1999) 2834–2839. doi:http://dx.doi.org/10.1063/1.873240.
URL http://scitation.aip.org/content/aip/journal/pop/6/7/10.1063/1.873240

[11] O. Sauter, C. Angioni, Y. R. Lin-Liu, Erratum: neoclassical conductivity and bootstrap current formulas for general axisymmetric equilibria and arbitrary collisionality regime [phys. plasmas 6, 2834 (1999)], Physics of Plasmas (1994-present) 9 (12) (2002) 5140–5140. doi:http://dx.doi.org/10.1063/1.1517052.
URL http://scitation.aip.org/content/aip/journal/pop/9/12/10.1063/1.1517052

[12] H. P. Summers, W. J. Dickson, M. G. O'Mullane, N. R. Badnell, A. D. Whiteford, D. H. Brooks, J. Lang, S. D. Loch, D. C. Griffin, Ionization state, excited populations and emission of impurities in dynamic finite density plasmas: I. the generalized collisional-radiative model for light elements., Plasma Phys. Control. Fusion 48 (2) (2006) 263–293.

[13] M. Arnaud, R. Rothenflug, An updated evaluation of recombination and ionization rates, Astron. & Astrophys. Supp. Ser. 60 (1985) 425–457.

[14] Arnaud, Raymond, Astrophys. J 398.

[15] H. P. Summers, Tables and graphs of collisional dielectronic recombination and ionisation equilibra of h-like to a-like ions of elements, 367, Appleton Laboratory (1974).

[16] H. P. Summers, Atomic Data and Analysis Structure User Manual, version 2.6 (2007).

[17] T. Pütterich, R. Neu, R. Dux, A. Whiteford, M. O'Mullane, H. Summers, the ASDEX Upgrade Team, Calculation and experimental test of the cooling factor of tungsten, Nuclear Fusion 50 (2) (2010) 025012.
URL http://stacks.iop.org/0029-5515/50/i=2/a=025012

[18] S. D. Loch, J. A. Ludlow, M. S. Pindzola, A. D. Whiteford, D. C. Griffin, Electron-impact ionization of atomic ions in the w isonuclear sequence, Phys. Rev. A 72 (2005) 052716. doi:10.1103/PhysRevA.72.052716.
URL http://link.aps.org/doi/10.1103/PhysRevA.72.052716

[19] T. Pütterich, R. Neu, R. Dux, A. D. Whiteford, M. G. O'Mullane, et al., Modelling of measured tungsten spectra from asdex upgrade and predictions for iter, Plasma Phys. Contr. Fusion 50 (8) (2008) 085016.

[20] Fidone, Giruzzi, Granata, Synchrotron radiation loss in tokamaks of arbitrary geometry, Nucl. Fusion 41 (12) (2001) 1755.

[21] Albajar, Johner, Granata, Improved calculation of synchrotron radiation losses in realistic tokamak plamsas, Nucl. Fusion 41 (6) (2001) 665.

[22] I. P. E. G. on Confinement, Transport, I. P. E. G. on Confinement Modelling, Database, I. P. B. Editors, Chapter2: Plasma confinement and transport, Nuclear Fusion 39 (12) (1999) 2175.
URL http://stacks.iop.org/0029-5515/39/i=12/a=302

[23] H. Zohm, C. Angioni, E. Fable, G. Federici, G. Gantenbein, T. Hartmann, K. Lackner, E. Poli, L. Porte, O. Sauter, G. Tardini, D. Ward, M. Wischmeier, On the physics guidelines for a tokamak demo, Nuclear Fusion 53 (7) (2013) 073019.
URL http://stacks.iop.org/0029-5515/53/i=7/a=073019

[24] R. Kemp, E. Fable, H. Lux, R. Wenninger, Radiation and confinement in 0-d fusion system codes, in prep.

[25] D. Boucher, Iter physics design description document, Tech. rep. (1996).

[26] J. A. Snipes, Iter h-mode threshold database working group, in: Controlled Fusion and Plasma Physics, 24th EPS Conference, Berchtesgaden, Vol. 21A, part III, 1997, p. 961.

[27] Y. R. Martin, T. Takizuka, the ITPA CDBM H-mode Threshold Database Working Group, Power requirement for accessing the h-mode in iter, Journal of Physics: Conference Series 123 (1) (2008) 012033.
URL http://stacks.iop.org/1742-6596/123/i=1/a=012033

[28] A. Kallenbach, M. Bernert, R. Dux, L. Casali, T. Eich, et al., Impurity seeding for tokamak power exhaust: from present devies via iter to demo, Plasma Phys. Control. Fusion 55 (2013) 124041.

[29] P. Carolan, V. Piotrowicz, The behaviour of impurities out of coronal equilibrium, Plasma Physics 25 (10) (1983) 1065.

[30] K. Behringer, Description of the impurity transport code strahl, Tech. Rep. JET-R(87)08, JET Joint Undertaking, Culham (1987).

[31] R. Dux, Laborbericht 10/30, Tech. rep., IPP Garching (2006).

[32] M. Sertoli, C. Angioni, R. Dux, R. Neu, T. Ptterich, V. Igochine, the ASDEX Upgrade Team, Local effects of ecrh on argon transport in l-mode discharges at asdex upgrade, Plasma Physics and Controlled Fusion 53 (3) (2011) 035024.
URL http://stacks.iop.org/0741-3335/53/i=3/a=035024

[33] L. Casali, E. Fable, R. Dux, M. Bernert, R. Fischer, A. Kallenbach, et al., Transport analysis and modelling of high radiation and high density plasmas at asdex upgrade, in: 41st EPS Conference on Controled Fusion and Plasma Physics, 2014.

[34] K. Lackner, Figures of merit for divertor similarity, Comments Plasma Phys. Contr. Fus. 15 (6) (1994) 359–365.
[35] T. Eich, B. Sieglin, A. Scarabosio, W. Fundamenski, R. J. Goldston, A. Herrmann, Inter-elm power decay length for jet and asdex upgrade: Measurement and comparison with heuristic drift-based model, Phys. Rev. Lett. 107 (2011) 215001. doi:10.1103/PhysRevLett.107.215001.
URL http://link.aps.org/doi/10.1103/PhysRevLett.107.215001
[36] H. Zohm, Assessment of {DEMO} challenges in technology and physics, Fusion Engineering and Design 88 (68) (2013) 428 – 433, proceedings of the 27th Symposium On Fusion Technology (SOFT-27); Lige, Belgium, September 24-28, 2012. doi:http://dx.doi.org/10.1016/j.fusengdes.2013.01.001.
URL http://www.sciencedirect.com/science/article/pii/S0920379613000021
[37] A. Kallenbach, M. Bernert, M. Beurskens, L. Casali, T. Eich, L. Giannone, A. Herrmann, M. Maraschek, et al., Partial detachment of high power discharges in asdex upgrade, in: IAEA 2014 Proceedings.
[38] N. Uckan, I. P. Group, Iter physics design guidelines: 1989, Tech. rep., IAEA, Vienna, iTER Documentation Series, No. 10 (1990).
[39] R. Dux, A. Loarte, E. Fable, A. Kukushkin, Transport of tungsten in the h-mode edge transport barrier of iter, Plasma Physics and Controlled Fusion.
[40] F. Casson, R. McDermott, C. Angioni, Y. Camenen, R. Dux, E. Fable, R. Fischer, B. Geiger, P. Manas, L. Menchero, G. Tardini, the ASDEX Upgrade Team, Validation of gyrokinetic modelling of light impurity transport including rotation in asdex upgrade, Nuclear Fusion 53 (6) (2013) 063026.
URL http://stacks.iop.org/0029-5515/53/i=6/a=063026
[41] R. M. McDermott, C. Angioni, R. Dux, E. Fable, T. Ptterich, F. Ryter, A. Salmi, T. Tala, G. Tardini, E. Viezzer, the ASDEX Upgrade Team, Core momentum and particle transport studies in the asdex upgrade tokamak, Plasma Physics and Controlled Fusion 53 (12) (2011) 124013.
URL http://stacks.iop.org/0741-3335/53/i=12/a=124013
[42] B. Lipschultz, B. LaBombard, E. Marmar, M. Pickrell, J. Terry, R. Watterson, S. Wolfe, Marfe: an edge plasma phenomenon, Nuclear Fusion 24 (8) (1984) 977.
URL http://stacks.iop.org/0029-5515/24/i=8/a=002
[43] C. Reux, F. Imbeaux, J.-F. Artaud, P. Bernardi, J. B. et al., Sycomore: a modular system code for demo reactor design, Poster at 2nd IAEA DEMO Programme Workshop, Vienna, Austria. (December 2013).
[44] H. P. Summers, R. W. P. McWhirter, Radiative power loss from laboratory and astrophysical plasmas. i. power loss from plasmas in steady-state ionisation balance 12 (14) (1979) 2387–2412. doi:10.1088/0022-3700/12/14/022.
[45] J. Artaud, V. Basiuk, F. Imbeaux, M. Schneider, J. G. et al., The cronos suite of codes for integrated tokamak modelling, Nuclear Fusion 50 (4) (2010) 043001.
URL http://stacks.iop.org/0029-5515/50/i=4/a=043001
[46] G. Giruzzi, J. Artaud, T. Bolzonella, E. Fable, L. G. et al., Scenario modelling, Tech. rep., EFDA-Power Plant Physics & Technology, wP13-SYS01B-D06 (December 2013).
[47] S. Wiesen, Jintrac - jet modelling suite, Tech. rep., JET (2008).
[48] W. A. Houlberg, et al., Phys. Plasmas 4 (1997) 3230.
[49] M. Reinke, Challenges to radiative divertor/mantle operations in advanced, steady-state scenarios, in: Proceedings of the 7th IAEA Technical Meeting on Steady State Operation of Magnetic Fusion Devices, no. PSFC/RR-13-11, 2013.
URL http://www.psfc.mit.edu/library1/catalog/reports/2010/13rr/13rr011/13rr011_abs.html
[50] W. Biel, M. de Baar, A. Dinklage, F. Felici, R. Knig, H. Meister, W. Treutterer, R. Wenninger, Demo diagnostics and burn control, in: 28th SOFT Proceedings, 2014.
[51] R. Wenninger, M. Bernert, T. Eich, E. Fable, G. Federici, A. Kallenbach, A. Loarte, C. Lowry, D. McDonald, R. Neu, T. Ptterich, P. Schneider, B. Sieglin, G. Strohmayer, F. Reimold, M. Wischmeier, Demo divertor limitations during and in between elms, Nuclear Fusion 54 (11) (2014) 114003.
URL http://stacks.iop.org/0029-5515/54/i=11/a=114003
[52] J. Rapp, T. Eich, M. von Hellermann, A. Herrmann, L. C. Ingesson, S. Jachmich, G. F. Matthews, V. Philipps, G. Saibene, contributors to the EFDA-JET Workprogramme, Elm mitigation by nitrogen seeding in the jet gas box divertor, Plasma Physics and Controlled Fusion 44 (6) (2002) 639.
URL http://stacks.iop.org/0741-3335/44/i=6/a=302
[53] F. Reimold, M. Wischmeier, M. Bernert, S. Potzel, A. Kallenbach, H. Müller, B. Sieglin, U. Stroth, the ASDEX Upgrade Team, Divertor studies in nitrogen induced, completely detached h-modes in full tungsten asdex upgrade, Nuclear Fusion submitted.
[54] A. Huber, M. Wischmeier, C. Lowry, S. Brezinsek, et al., Impact of strong impurity seeding on the the radiation losses in jet with iter-like wall, in: 41st EPS Conference on Controled Fusion and Plasma Physics, 2014.
[55] M. Wischmeier, High density operation for reactor-relevant power exhaust, Journal of Nuclear Materials (0) (2014) –. doi:http://dx.doi.org/10.1016/j.jnucmat.2014.12.078.
URL http://www.sciencedirect.com/science/article/pii/S0022311514
[56] A. Kallenbach, M. Bernert, T. Eich, J. Fuchs, L. Giannone, et al., Optimized tokamak power exhaust with double radiative feedback in asdex upgrade, Nuclear Fusion 52 (12) (2012) 122003.
URL http://stacks.iop.org/0029-5515/52/i=12/a=122003
[57] D. J. Ward, R. Kemp, The resilience of an operating point for a fusion power plant, in: SOFT 2014 Proceedings.